OPEN ACCESS

Int. Jr. of Contemp. Res. in Multi. *PEER-REVIEWED JOURNAL* *Volume 5 Issue 3 [May-Jun] Year 2026*

Research Article

A Study of Major Geomagnetic Storms in Relation to Solar and Interplanetary Magnetic Fields During Solar Cycle 24

Kirti Maurya [1], G N Singh [2], Lokesh Ojha [3], CM Tiwari [4], Sandeep Kumar Tiwari [5*]

[1, 3, 4] Department of Physics, Awadhesh Pratap Singh University, Rewa, Madhya Pradesh, India

[2] Department of Physics, Sudarshan College, Lalgaon, Rewa, Madhya Pradesh, India

[5] Department of Physics, Govt Model Science College, Rewa, Madhya Pradesh, India

Corresponding Author: * Sandeep Kumar Tiwari

DOI: https://doi.org/10.5281/zenodo.20395545

Abstract

Geomagnetic storms are major disturbances in Earth's magnetosphere caused by interactions between solar wind plasma, interplanetary magnetic field (IMF) structures, and Earth's magnetic field. This study investigates the relationship between geomagnetic activity, solar wind parameters, IMF variations, and galactic cosmic ray intensity (CRI) during two major geomagnetic storms of solar cycle 24: 14-17 March 2015 and 22-23 June 2015. Hourly solar wind velocity, plasma density, IMF Scalar B, and Bz data were obtained from the OMNI database, while CRI measurements were acquired from the Oulu Neutron Monitor. The Disturbance Storm Time (Dst) index was used as the primary indicator of geomagnetic storm intensity. Correlation and regression analyses were applied to evaluate the geoeffectiveness of CME-driven interplanetary disturbances.

The March 2015 storm was associated with a fast Earth-directed coronal mass ejection (CME) and prolonged southward IMF Bz conditions. Moderate positive correlations were observed between Dst and IMF Bz (r = 0.596) and solar wind proton density (r = 0.575), whereas solar wind plasma velocity showed a moderate negative correlation (r = -0.431). A strong positive correlation between Dst and CRI (r = 0.831) confirmed a significant Forbush decrease during the storm interval. In contrast, the June 2015 storm was dominated by high solar wind velocity and interacting CME-driven shock structures. The strongest relationship was observed between Dst and solar wind plasma velocity (r = -0.914), indicating that solar wind speed was the dominant interplanetary driver. Cosmic ray intensity also showed a strong positive correlation with Dst (r = 0.910), revealing substantial cosmic ray modulation associated with CME turbulence and shock-compressed sheath regions.

The comparative analysis demonstrates that geomagnetic storm intensity during solar cycle 24 depended on IMF orientation, solar wind velocity, plasma density, and CME sheath dynamics. Both storms produced significant Forbush decreases, highlighting the strong coupling between CME-driven interplanetary disturbances and galactic cosmic ray modulation. The findings improve understanding of solar wind-magnetosphere interactions and contribute to space weather forecasting and prediction of geomagnetic storm impacts on near-Earth space environments.

Manuscript Information

- **ISSN No:** 2583-7397
- **Received:** 06-04-2026
- **Accepted:** 23-05-2026
- **Published:** 26-05-2026
- **IJCRM:**5(3); 2026: 394-405

- **Plagiarism Checked:** Yes
- **Peer Review Process:** Yes

How to Cite this Article

Maurya K, Singh G N, Ojha L, Tiwari C M, Tiwari S K. A Study of Major Geomagnetic Storms in Relation to Solar and Interplanetary Magnetic Fields During Solar Cycle 24. Int J Contemp Res Multidiscip. 2026;5(3):394-405.

Access this Article Online

www.multiarticlesjournal.com

KEYWORDS: Solar Cycle 24, Geomagnetic Storms, Interplanetary Magnetic Field (Bz), Coronal Mass Ejections (CMEs), Forbush Decrease, Space Weather, Dst Index.

1. INTRODUCTION

Geomagnetic storms represent the most profound and dynamic disturbances in the Earth's magnetosphere, primarily driven by the complex coupling between solar ejecta and the terrestrial magnetic field. The observational foundation of extreme space weather traces back to the mid-19th century, notably the Carrington Event, which provided the first direct link between catastrophic white-light solar flares and subsequent severe global magnetic disturbances and auroral displays (Carrington, 1859; Hodgson, 1859; Loomis, 1861) [6, 14, 19]. Since these early historical observations, understanding the physical mechanisms that trigger such immense energy transfers has become a cornerstone of solar-terrestrial physics. Recent investigations have further emphasized the role of solar wind structures, interplanetary magnetic field variations, and transient solar eruptive phenomena in modulating geomagnetic activity and cosmic ray intensity during modern solar cycles (Baghel *et al*., 2026; Dwivedi *et al*., 2026a; Tiwari *et al*., 2026a) [1, 7, 29].

The primary requirement for the transfer of solar wind energy into the magnetosphere is the process of magnetic reconnection. This process is highly dependent on a strong and sustained southward component of the interplanetary magnetic field (Bz) (Rostoker & Falthammar, 1967; Tsurutani & Meng, 1972; Rawat *et al*., 2018) [27, 23, 32]. Empirical relationships established over decades demonstrate that when these specific interplanetary conditions are met, solar wind energy is efficiently injected into the inner magnetosphere. This drives intense ring currents that cause significant global depressions in the Earth's magnetic field, which are quantified by the Disturbance Storm Time (Dst) index (Burton *et al*., 1975; Gonzalez & Tsurutani, 1987; Iyemori, 1990) [4, 10, 15]. Recent studies have also shown that variations in solar wind speed, plasma density, and IMF structures strongly influence cosmic ray modulation and geomagnetic storm intensity during Solar Cycles 24 and 25 (Baghel *et al*., 2026; Maurya *et al*., 2026) [1, 20].

Extensive statistical studies of previous solar cycles have identified two primary classes of interplanetary drivers responsible for intense (Dst ≤ -100 nT) and superintense (Dst ≤ -250 nT) geomagnetic storms. Near solar maximum, the dominant drivers are transient phenomena, specifically Interplanetary Coronal Mass Ejections (ICMEs) and their preceding shock-compressed sheath regions or internal magnetic clouds (Tsurutani *et al*., 1988; Gonzalez *et al*., 1989; Echer *et al*., 2008b) [35, 12, 9]. During the declining phase of the solar cycle, fast solar wind streams originating from coronal holes interact with slower streams to form Corotating Interaction Regions (CIRs) and Stream Interaction Regions (SIRs). These regions frequently trigger recurrent, albeit sometimes less severe, magnetic storms (Tsurutani *et al*., 1995a, 1995b) [33, 34]. The morphological development of these storms can be highly complex, often exhibiting a two-step main phase dictated by the sequential interaction of differing interplanetary magnetic structures (Kamide *et al*., 1998) [16]. Contemporary analyses further demonstrate that CME propagation characteristics and heliospheric solar wind features significantly influence periodic and transient cosmic ray variations across Solar Cycle 24 (Dwivedi *et al*., 2026b; Tiwari *et al*., 2026b) [8, 30].

Understanding the boundaries of extreme space weather has gained critical importance due to the severe vulnerability of modern technological infrastructure to geomagnetically induced currents (Bolduc, 2002; National Research Council Report, 2008; Hapgood, 2012; Lakhina *et al*., 2012) [3, 21, 13, 18]. Models of Carrington-like storms and analyses of contemporary extreme events such as the Halloween Storms of 2003 and the anomalous July 2012 solar eruptive event highlight how rapidly these drivers can propagate and impact the Geospace environment (Skoug *et al*., 2004; Tsurutani *et al*., 2012; Baker *et al*., 2013) [28, 36, 2]. Recent investigations have also highlighted the influence of geomagnetic storms on near-Earth space weather conditions during the ascending phase of Solar Cycle 24 and the role of solar eruptive events in cosmic ray enhancement phenomena (Tiwari *et al*., 2026c; Tiwari *et al*., 2024) [31].

Against this extensive theoretical and historical backdrop, Solar Cycle 24 presented a distinctly anomalous heliospheric environment. The cycle commenced in late 2008 following a prolonged minimum and was marked by a ~30% reduction in sunspot activity compared to Solar Cycle 23, making it one of the weakest cycles in modern observational history (Richardson, 2013) [25]. Due to these weakened solar conditions and an overall depression in the background interplanetary magnetic field, the occurrence rate of intense geomagnetic storms dropped by approximately 75% relative to the previous cycle (Rawat *et al*., 2018) [23]. However, the major storms that did occur such as the “St. Patrick’s Day Storm” of 2015 revealed critical insights into how lower ambient solar wind pressure alters the expansion and geoeffectiveness of transient solar drivers (Navia *et al*., 2018) [22]. Recent studies have additionally demonstrated that CME evolution, heliospheric magnetic field variations, and solar energetic particle propagation continued to significantly affect geomagnetic and cosmic ray environments during the later phases of Solar Cycle 24 and the onset of Solar Cycle 25 (Dwivedi *et al*., 2026a; Maurya *et al*., 2026) [7, 20].

Building upon the foundational criteria established for earlier cycles, this study investigates the major geomagnetic storms of Solar Cycle 24. By utilizing comprehensive solar wind parameters extracted from the OMNI database, we evaluate the exclusivity and geoeffectiveness of in situ interplanetary drivers within this weakened cycle. Furthermore, we examine the associated modulation of galactic cosmic ray intensity, analysing how the altered magnetic structures of Cycle 24 influenced the amplitude and recovery profiles of Forbush decreases during these major events. The study also complements recent investigations on solar wind variability, CME propagation, geomagnetic storm dynamics, and cosmic ray modulation during contemporary solar cycles (Baghel *et al*., 2026; Dwivedi *et al*., 2026b; Tiwari *et al*., 2026b) [1, 8, 30].

2. DATA AND METHODOLOGY

To conduct a robust statistical and morphological analysis of the geomagnetic and interplanetary conditions, this study

utilizes high-resolution (Hourly) observational data from multiple primary sources:

1. **OMNI Database:** Time-shifted in situ measurements of solar wind plasma and IMF parameters at Earth's bow shock were extracted from the OMNI database. Key parameters analysed include solar wind velocity (Vsw), plasma density, total magnetic field magnitude (B), and the critical southward magnetic field component (Bz).
2. **Oulu Neutron Monitor:** To evaluate the modulation of galactic cosmic rays and track variations in cosmic ray intensity (CRI), ground-level neutron count data were obtained from the high-latitude Oulu Neutron Monitor facility.
3. **SOHO/LASCO CME catalogue:** Coronal mass ejection (CME) characteristics, including CME onset time, angular width, propagation speed, and halo structure, were obtained from the SOHO/LASCO CME catalogue. These observations were used to identify Earth-directed CMEs associated with the investigated geomagnetic storms.
4. **GOES Solar Flare Database:** Solar flare information, including flare class, onset time, peak intensity, and active region identification, was obtained from the GOES X-ray flare catalogue. These data were used to examine the solar eruptive events associated with CME initiation and subsequent geomagnetic disturbances.

The primary metric for storm classification is the Disturbance Storm Time (Dst) index, derived from a network of low-latitude magnetometer stations. Storms during Solar Cycle 24 are classified based on the minimum Dst achieved during the main phase:

- Moderate Storms: -100 nT < Dst ≤ -50 nT
- Intense (Major) Storms: Dst ≤ -100 nT

Superposed epoch analysis and correlational methodologies were applied to synchronize the onset of the in situ interplanetary drivers with the main phase of the Dst index depression and the corresponding decrease in cosmic ray intensity.

3. RESULTS AND DISCUSSION

This study investigates the interrelationship between geomagnetic disturbances, interplanetary magnetic field (IMF) variations, solar wind plasma parameters, and galactic cosmic ray intensity (CRI) during two major geomagnetic storms of Solar Cycle 24: the 14-17 March 2015 "St. Patrick's Day Storm" and the 22-23 June 2015 "Summer Solstice Storm." Correlation and regression analyses were performed using the Dst index as the primary geomagnetic indicator to evaluate the geoeffectiveness of CME-driven interplanetary disturbances.

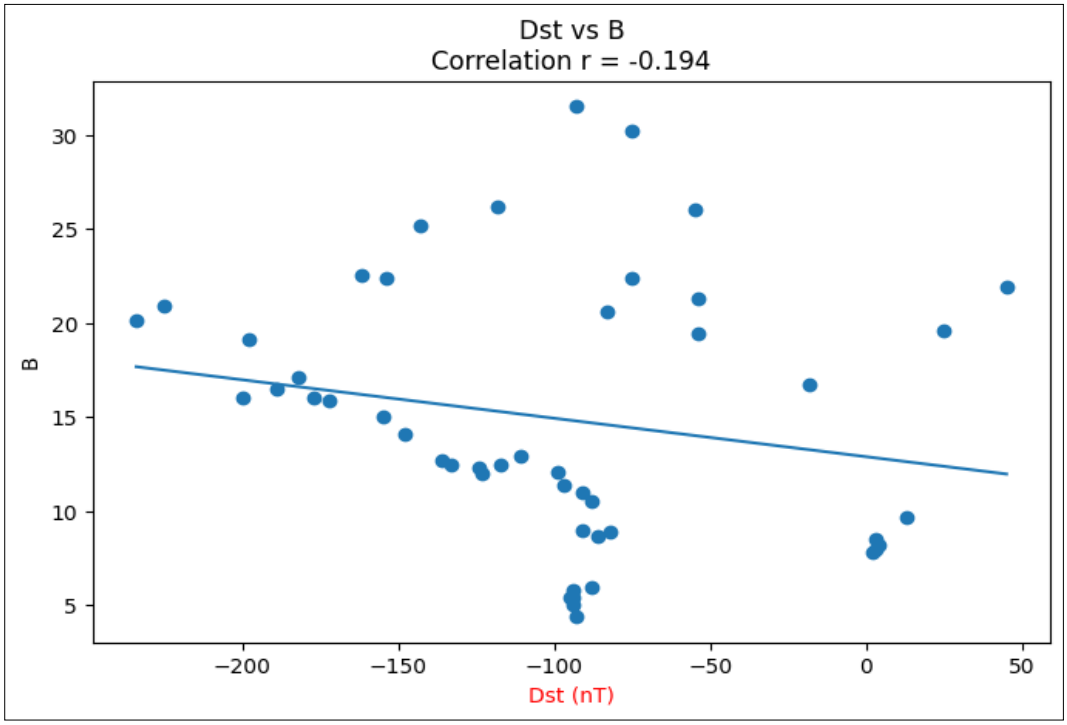

Fig 3.1 Scatter plot showing the relationship between Dst index (nT) and Scalar B nT during the geomagnetic storm of 14-17 March 2015. The regression line indicates a weak negative correlation (r = -0.194) between the two parameters.

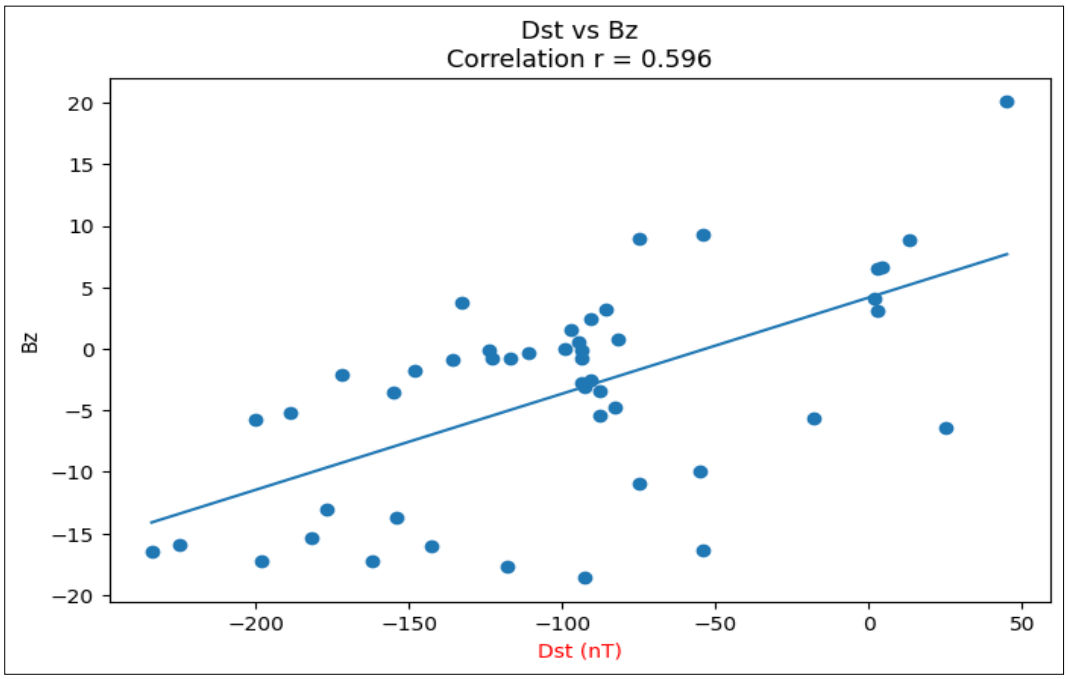

Fig 3.2 Scatter plot showing the relationship between Dst index (nT) and Bz nT during the geomagnetic storm of 14-17 March 2015. The regression line indicates a moderate positive correlation (r = 0.596) between the two parameters.

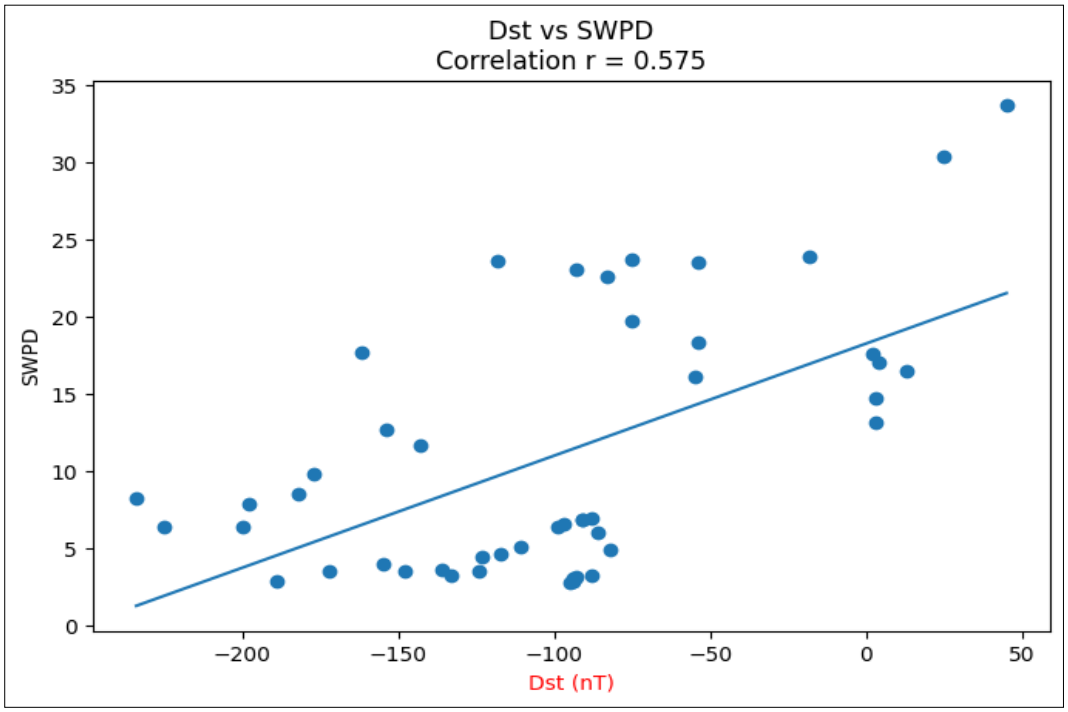

Fig 3.3: Scatter plot showing the relationship between Dst index (nT) and SWPD N/cm^3 during the geomagnetic storm of 14-17 March 2015. The regression line indicates a moderate positive correlation (r = 0.575) between the two parameters.

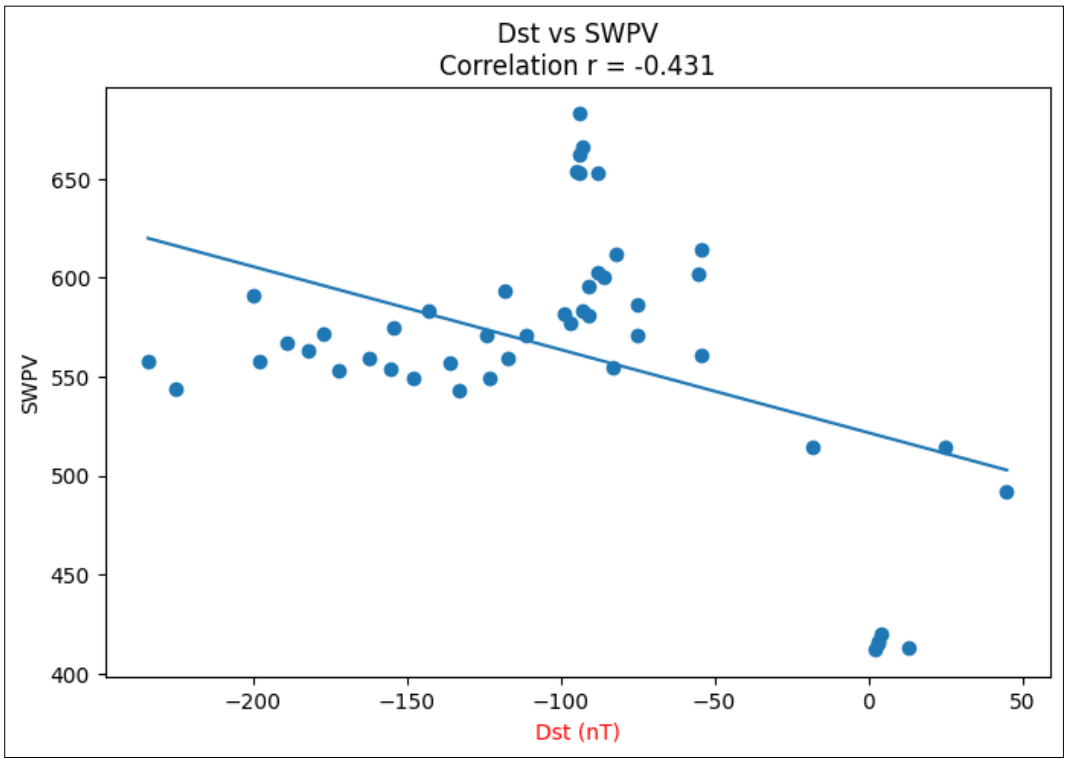

Fig 3.4: Scatter plot showing the relationship between Dst index (nT) and SWPV km/s during the geomagnetic storm of 14-17 March 2015. The regression line indicates a moderate negative correlation (r = -0.431) between the two parameters.

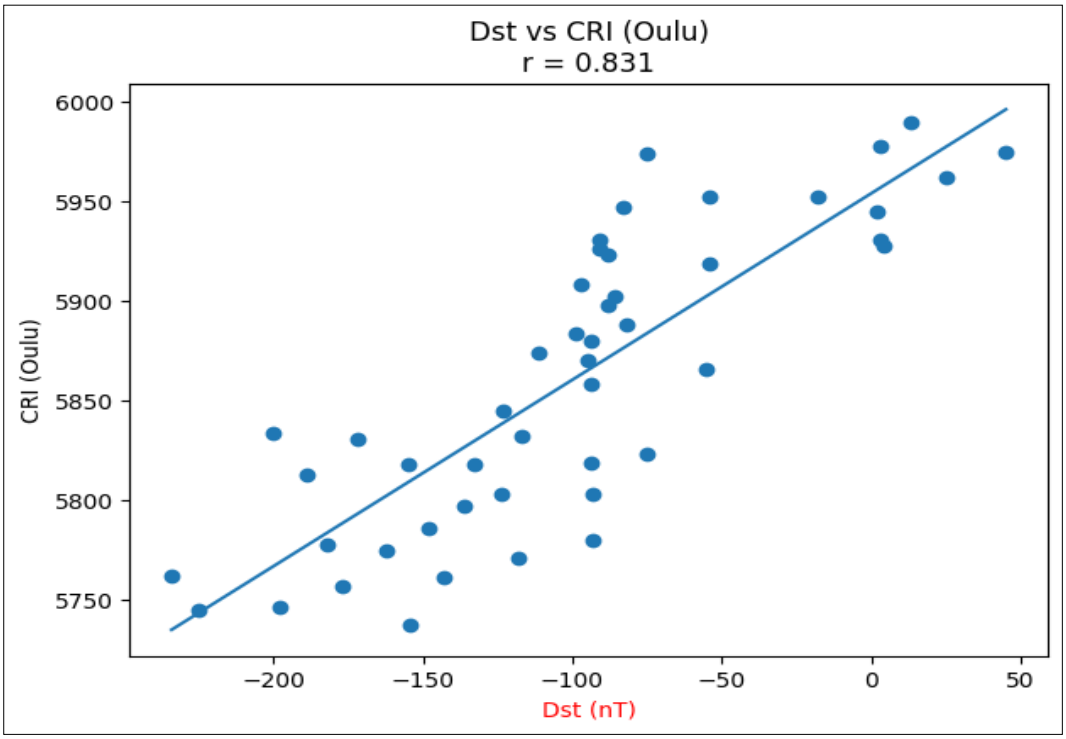

Fig 3.5: Scatter plot showing the relationship between Dst index (nT) and CRI (Oulu) during the geomagnetic storm of 14-17 March 2015. The regression line indicates a strong positive correlation (r = 0.831) between the two parameters.

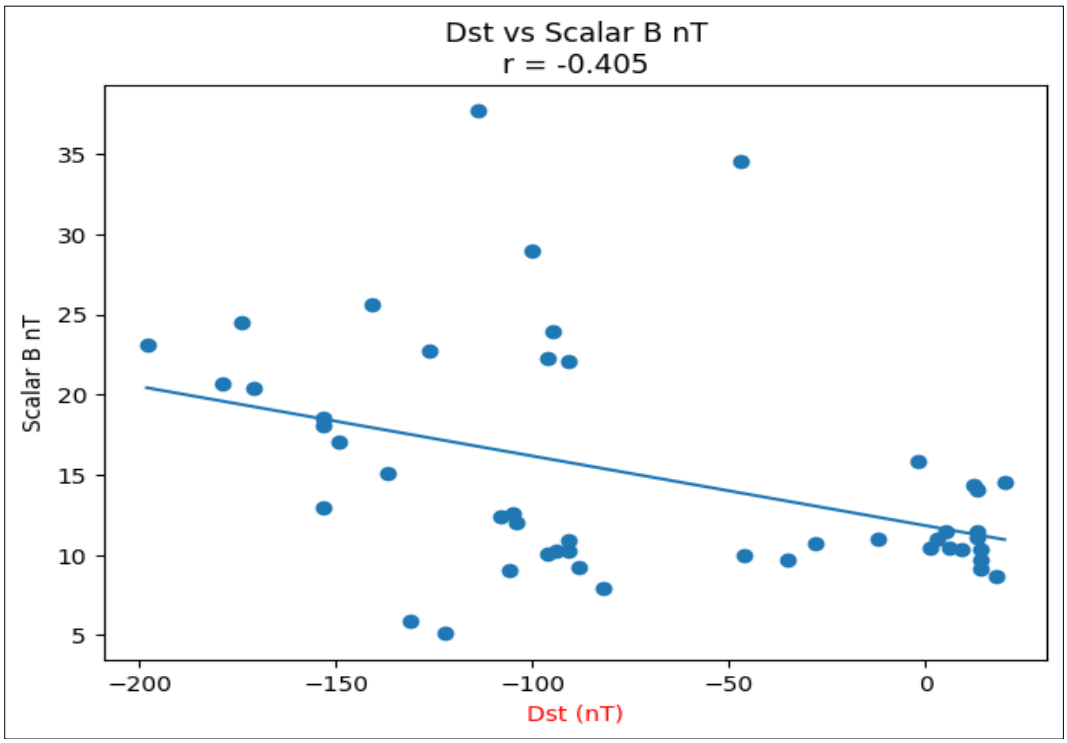

Fig 3.5: Scatter plot illustrating the correlation between Dst index (nT) and total interplanetary magnetic field strength (Scalar B, nT) during the geomagnetic storm of 22-23 June 2015. The regression analysis reveals a moderate negative correlation (r = -0.405) between geomagnetic disturbance intensity and IMF magnitude.

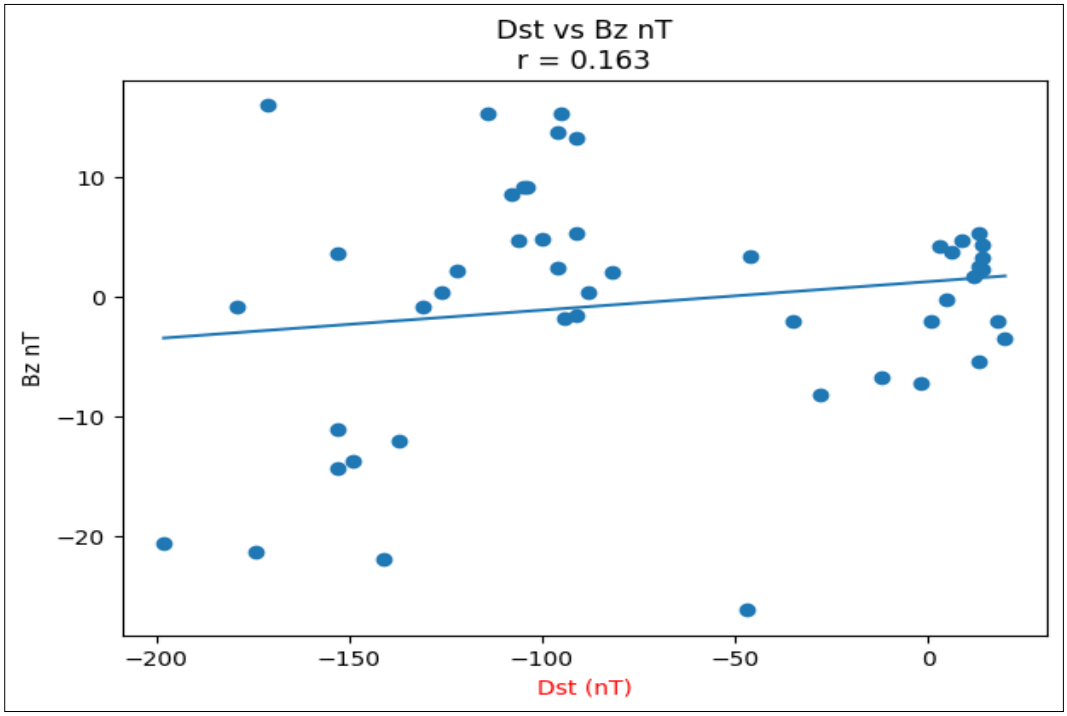

Fig 3.6 Scatter plot between Dst index (nT) and southward interplanetary magnetic field component (Bz, nT) during the geomagnetic storm of 22-23 June 2015. The regression line indicates a weak positive correlation (r = 0.163) during the analysed interval.

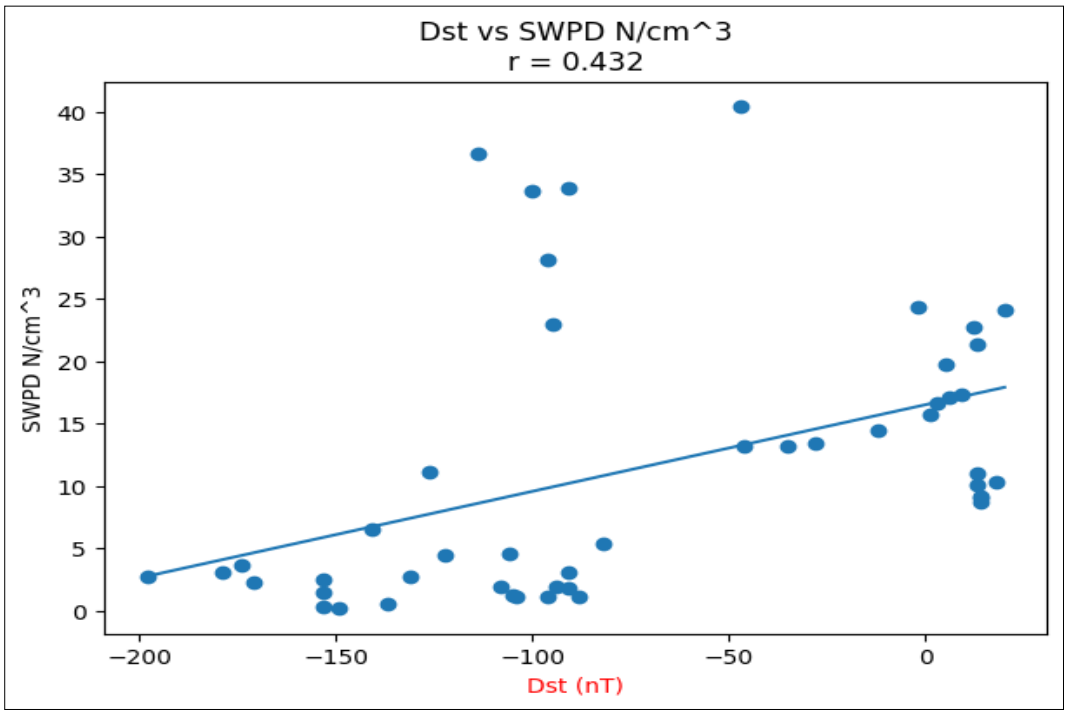

Fig 3.7: Scatter plot showing the relationship between Dst index (nT) and solar wind proton density (SWPD, N/cm³) during the geomagnetic storm of 22-23 June 2015. The fitted regression line demonstrates a moderate positive correlation (r = 0.432) between plasma density enhancement and geomagnetic activity.

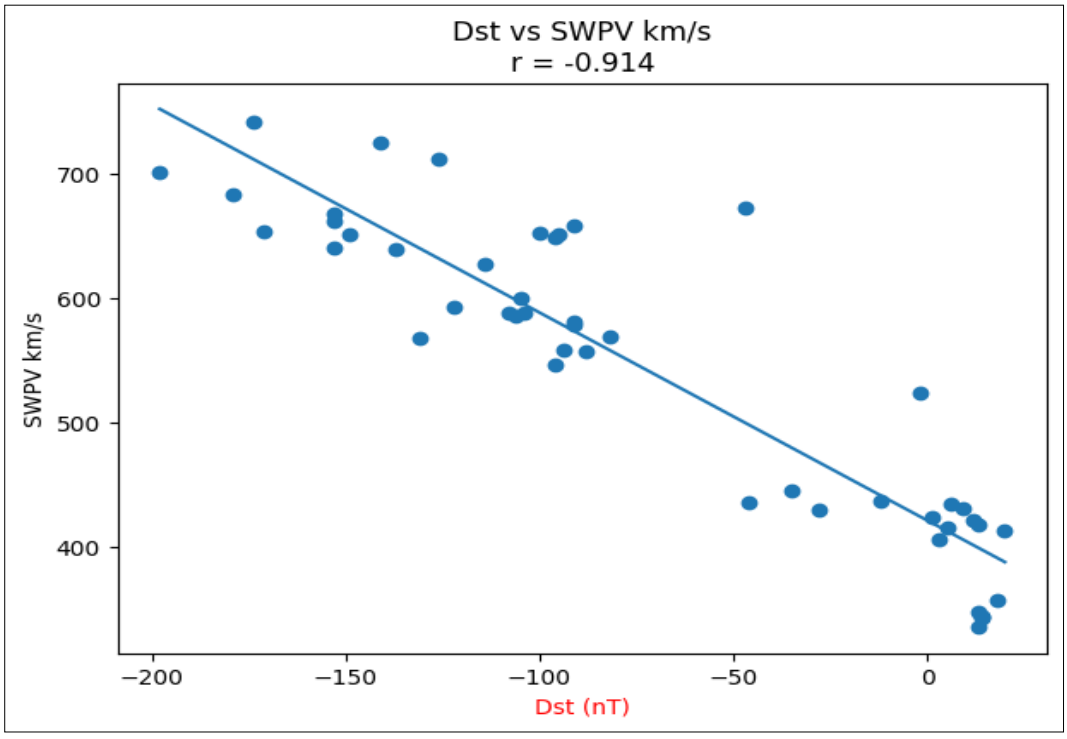

Fig 3.8: Scatter plot illustrating the relationship between Dst index (nT) and solar wind plasma velocity (SWPV, km/s) during the geomagnetic storm of 22-23 June 2015. The regression analysis indicates a strong negative correlation (r = -0.914), suggesting significant influence of solar wind speed on geomagnetic storm intensity.

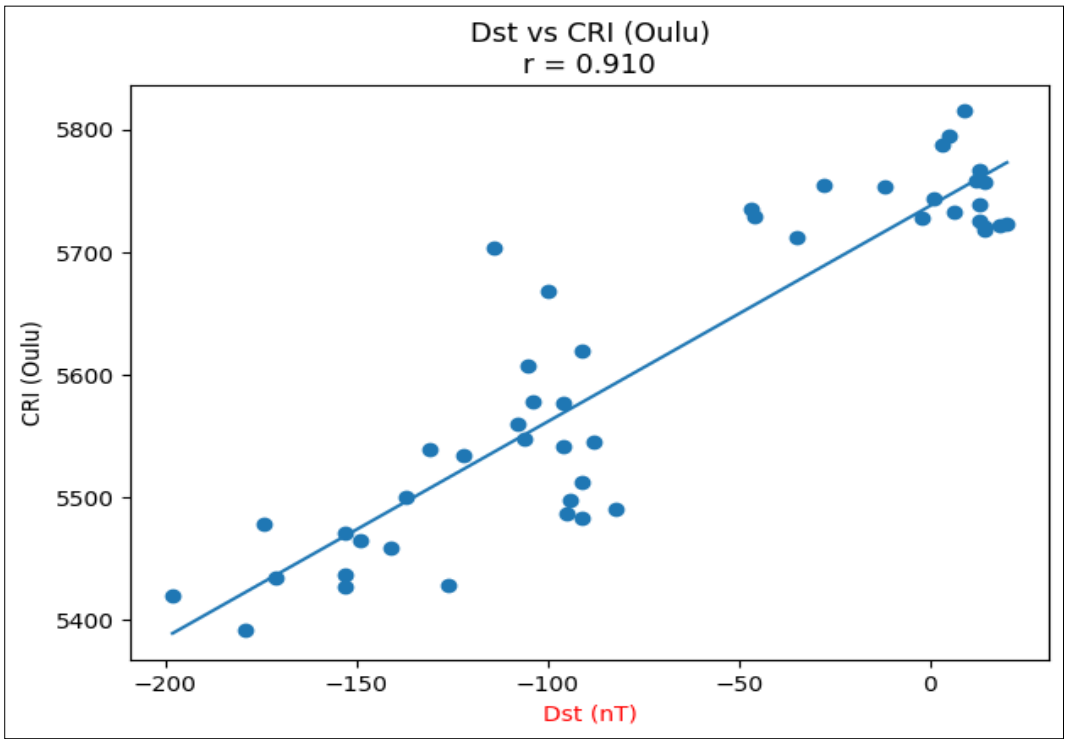

Fig 3.9: Scatter plot between Dst index (nT) and cosmic ray intensity measured at Oulu neutron monitor (CRI) during the geomagnetic storm of 22-23 June 2015. The regression line shows a strong positive correlation (r = 0.910), indicating close association between geomagnetic disturbances and cosmic ray variations during the event.

Table 3.1: Contains calculated correlation coefficients, regression slope and regression intercept between Dst and other selected parameters during the geomagnetic storm of 14-17 March 2015.

Parameter	Correlation Coefficient (r)	Regression Slope	Regression Intercept
Scalar B nT	-0.1944	-0.0204	12.8999
Bz nT	0.5958	0.0781	4.1748
SWPD N/cm^3	0.5746	0.0727	18.2609
SWPV km/s	-0.4306	-0.4201	521.6778
CRI (Oulu)	0.8306	0.9364	5954.0503

Table 3.2: Contains calculated correlation coefficients, regression slope and regression intercept between Dst and other selected Parameters during the geomagnetic storm of 22-23 June 2015.

Parameter	Correlation Coefficient (r)	Regression Slope	Regression Intercept
Scalar B nT	-0.4047	-0.0434	11.8196
Bz nT	0.1632	0.0238	1.2503
SWPD N/cm^3	0.4317	0.0694	16.5312
SWPV km/s	-0.9142	-1.6709	421.8266
CRI (Oulu)	0.9098	1.7619	5737.6343

3.1 Geomagnetic Storm of 14-17 March 2015

The geomagnetic storm of 14-17 March 2015 was initiated by a fast Earth-directed coronal mass ejection (CME) associated with a long-duration C9.1-class solar flare originating from NOAA Active Region (AR) 12297. The CME was observed by the SOHO/LASCO coronagraph as a partial halo CME at approximately 02:10 UT on 15 March 2015. The eruption was further accompanied by type II and type IV radio bursts, indicating the presence of strong shock acceleration mechanisms in the solar corona (Kataoka *et al*., 2015) [17].

Upon arrival at Earth on 17 March 2015, the CME interacted strongly with the terrestrial magnetosphere and produced the most intense geomagnetic storm of Solar Cycle 24, with Dst values decreasing below -200 nT. The storm evolution occurred in two phases due to complex interplanetary magnetic field (IMF) structures and prolonged southward IMF Bz intervals.

IMF and Solar Wind Characteristics

Figure 3.1 illustrates the relationship between Dst and IMF Scalar B during the storm interval. A weak negative correlation (r = -0.194) was observed, indicating that although IMF enhancement contributed to geomagnetic activity, the total magnetic field magnitude alone was insufficient to determine storm intensity.

Figure 3.2 presents the correlation between Dst and the southward IMF component (Bz). The moderate positive correlation (r = 0.596) demonstrates that sustained southward Bz conditions played a dominant role in facilitating magnetic

reconnection and energy transfer into Earth's magnetosphere. Southward Bz intervals are widely recognized as one of the principal drivers of intense geomagnetic storms (Gonzalez *et al*., 1994) [11].

Similarly, Figure 3.3 shows a moderate positive correlation (r = 0.575) between Dst and solar wind proton density (SWPD). Enhanced plasma density within the CME sheath region increased solar wind dynamic pressure and intensified magnetospheric compression.

Figure 3.4 demonstrates a moderate negative correlation (r = -0.431) between Dst and solar wind plasma velocity (SWPV). This indicates that elevated solar wind speeds associated with the CME contributed significantly to ring current enhancement and storm intensification.

Cosmic Ray Modulation

A strong positive correlation (r = 0.831) was observed between Dst and cosmic ray intensity (CRI) measured at the Oulu Neutron Monitor, as shown in Figure 3.5. The pronounced reduction in cosmic ray intensity confirms the occurrence of a significant Forbush decrease during the storm period. The expanding CME magnetic cloud and turbulent shock sheath acted as an efficient magnetic barrier that scattered incoming galactic cosmic rays (Cane, 2000) [5].

Overall, the March 2015 storm was primarily governed by the combined effects of sustained southward IMF Bz, enhanced solar wind velocity, and compressed CME sheath structures, which enabled efficient solar wind-magnetosphere coupling.

3.2 Geomagnetic Storm of 22-23 June 2015

The geomagnetic storm of 22-23 June 2015, often referred to as the "Summer Solstice Storm," was triggered by multiple Earth-directed CMEs associated with NOAA Active Region 2371. This active region produced several M-class solar flares and successive CME eruptions during 18-21 June 2015 (Watari, 2017) [37].

The arrival of two interplanetary CME-driven shocks at Earth at approximately 05:45 UT and 18:38 UT on 22 June 2015 significantly enhanced solar wind velocity, plasma density, and IMF compression, resulting in a severe G4-class geomagnetic storm.

IMF and Solar Wind Characteristics

Figure 3.6 shows the relationship between Dst and IMF Scalar B during the June storm interval. A moderate negative correlation (r = -0.405) was obtained, indicating stronger IMF compression effects compared with the March event. The enhanced magnetic field magnitude likely resulted from interacting CME structures and compressed sheath regions.

In contrast, Figure 3.7 reveals a weak positive correlation (r = 0.163) between Dst and IMF Bz. Unlike the March storm, the June event was not solely controlled by prolonged southward Bz conditions. Instead, the storm intensity was more strongly influenced by solar wind plasma dynamics and shock compression.

Figure 3.8 demonstrates a moderate positive correlation (r = 0.432) between Dst and solar wind proton density, suggesting that compressed plasma environments contributed to enhanced magnetospheric compression and geomagnetic activity.

The strongest relationship was observed between Dst and solar wind plasma velocity (Figure 3.9), which exhibited a very strong negative correlation (r = -0.914). This result confirms that solar wind speed was the dominant interplanetary driver during the June 2015 storm. High-speed plasma flows intensified the convection electric field and significantly enhanced ring current injection processes.

Cosmic Ray Variations and Forbush Decrease

A strong positive correlation (r = 0.910) was observed between Dst and cosmic ray intensity measured at the Oulu neutron monitor. The June storm therefore produced a substantial Forbush decrease, indicating highly effective cosmic ray modulation by the CME-driven magnetic structures and turbulent interplanetary sheath regions.

The stronger CRI correlation observed during the June storm compared with the March storm suggests that interacting CME structures and enhanced turbulence increased the scattering efficiency of galactic cosmic rays in interplanetary space.

3.3 Comparative Interpretation of Both Storms

Although both geomagnetic storms occurred during the relatively weak Solar Cycle 24, they exhibited different interplanetary driving mechanisms and magnetospheric responses. The March 2015 storm was primarily controlled by sustained southward IMF Bz associated with a magnetic cloud structure, whereas the June 2015 storm was dominated by extreme solar wind velocity and interacting CME-driven shock structures.

The comparative analysis further demonstrates that geomagnetic storm intensity cannot be explained solely by IMF magnitude. Instead, the coupling efficiency between solar wind plasma and Earth's magnetosphere depends on the combined effects of IMF orientation, plasma density, solar wind velocity, and CME sheath turbulence.

Both storms produced significant Forbush decreases, confirming the close relationship between CME magnetic structures and galactic cosmic ray modulation. The observed strong correlations between Dst and CRI support the hypothesis that enhanced solar wind disturbances effectively reduce cosmic ray penetration into Earth's atmosphere through magnetic scattering and shielding processes (Richardson, 2004) [24].

3.4 Limitations of The Study

Despite providing significant insights into geomagnetic storm dynamics and cosmic ray modulation during Solar Cycle 24, the present study has certain limitations. The analysis was confined to only two major geomagnetic storm events of 2015, and inclusion of additional storm events from different phases of Solar Cycle 24 could yield more statistically comprehensive conclusions. The study primarily relied on time-shifted OMNI solar wind and interplanetary magnetic field (IMF) datasets near Earth's bow shock; therefore, localized upstream interplanetary variations may not have been fully represented. Furthermore, the cosmic ray intensity analysis was based solely

on observations from the Oulu Neutron Monitor, whereas the incorporation of multiple neutron monitor stations from different geomagnetic latitudes and cutoff rigidities would improve the global interpretation of cosmic ray modulation. The use of linear regression and Pearson correlation coefficients may also be insufficient to capture the nonlinear interactions between solar wind parameters and geomagnetic activity. In addition, the utilization of hourly averaged observational data may smooth short-duration fluctuations and transient structures within CME sheath regions. Finally, the study mainly focused on observational correlations and did not incorporate numerical magnetohydrodynamic (MHD) simulations or ring current models, which could provide a more detailed understanding of storm-time magnetospheric dynamics.

4. CONCLUSION

The present study examined the interrelationship between geomagnetic disturbances, interplanetary magnetic field (IMF) variations, solar wind plasma parameters, and galactic cosmic ray intensity (CRI) during the major geomagnetic storms of 14-17 March 2015 and 22-23 June 2015 of Solar Cycle 24. Correlation and regression analyses using the Dst index as the primary geomagnetic indicator revealed that both storms were strongly associated with Earth-directed coronal mass ejections (CMEs) and their corresponding interplanetary disturbances.

The results demonstrate that the geomagnetic storm of 14-17 March 2015 was primarily controlled by sustained southward IMF Bz conditions associated with the CME magnetic cloud structure. Moderate positive correlations between Dst and IMF Bz ($r = 0.596$) as well as solar wind proton density ($r = 0.575$) indicate that magnetic reconnection and enhanced solar wind dynamic pressure played dominant roles in storm intensification. The moderate negative correlation between Dst and solar wind plasma velocity ($r = -0.431$) further confirms the contribution of elevated solar wind speed to ring current enhancement and geomagnetic activity. A strong positive correlation between Dst and cosmic ray intensity ($r = 0.831$) revealed the occurrence of a significant Forbush decrease caused by the CME magnetic cloud and turbulent sheath region.

In contrast, the geomagnetic storm of 22-23 June 2015 exhibited different interplanetary driving characteristics. The June storm was dominated primarily by extremely high solar wind velocity and interacting CME-driven shock structures rather than prolonged southward IMF Bz conditions. The very strong negative correlation between Dst and solar wind plasma velocity ($r = -0.914$) indicates that solar wind speed was the most influential parameter controlling geomagnetic storm intensity during this event. Moderate correlations with IMF Scalar B ($r = -0.405$) and solar wind proton density ($r = 0.432$) suggest that IMF compression and plasma density enhancements within CME sheath regions significantly contributed to magnetospheric compression and geomagnetic disturbances. Furthermore, the strong positive correlation between Dst and cosmic ray intensity ($r = 0.910$) confirms the presence of a pronounced Forbush decrease and demonstrates the strong modulation of galactic cosmic rays by CME-driven interplanetary turbulence.

The comparative analysis of both storms highlights that geomagnetic storm intensity during Solar Cycle 24 cannot be explained solely by IMF magnitude. Instead, the geoeffectiveness of a storm depends on the combined influence of IMF orientation, solar wind velocity, plasma density, CME sheath turbulence, and interplanetary shock interactions. The March 2015 storm was mainly governed by prolonged southward IMF Bz intervals, whereas the June 2015 storm was dominated by extreme solar wind velocity and multiple interacting CME structures.

The study also confirms the close relationship between CME-driven geomagnetic storms and galactic cosmic ray modulation. Both events produced substantial Forbush decreases, demonstrating that expanding CME magnetic clouds and turbulent sheath regions act as effective magnetic barriers that suppress the penetration of galactic cosmic rays into Earth's atmosphere.

Overall, the findings emphasize the critical role of CME-driven interplanetary disturbances in controlling geomagnetic storm evolution and cosmic ray variability during Solar Cycle 24. The results contribute to a better understanding of solar wind-magnetosphere coupling processes and may assist in improving space weather forecasting and prediction of geomagnetic storm impacts on near-Earth space environments.

5. ACKNOWLEDGEMENT

The authors gratefully acknowledges the use of data from the OMNI database (NASA GSFC) and the Oulu Neutron Monitor (Sodankylä Geophysical Observatory) which made this analysis possible.

REFERENCES

1. Baghel AS, Chamadia PK, Tiwari CM, Tiwari SK. The influence of solar wind parameters and geomagnetic activity on cosmic ray intensity profiles. International Journal of Contemporary Research in Multidisciplinary. 2026;5(2):600-605. doi:10.5281/zenodo.19558760.
2. Baker DN, Li X, Pulkkinen A, Ngwira CM, Mays ML, Galvin AB, *et al*. A major solar eruptive event in July 2012: defining extreme space weather scenarios. Space Weather. 2013;11:585-591.
3. Bolduc L. GIC observations and studies in the Hydro-Quebec system. Journal of Atmospheric and Solar-Terrestrial Physics. 2002;64:1793.
4. Burton RK, McPherron RL, Russell CT. Empirical relationship between interplanetary conditions and Dst. Journal of Geophysical Research. 1975;80:4204.
5. Cane HV. Coronal mass ejections and Forbush decreases. Space Science Reviews. 2000;93:55-77.
6. Carrington RC. Description of a singular appearance seen in the Sun on September 1, 1859. Monthly Notices of the Royal Astronomical Society. 1859;20:13-15.
7. Dwivedi R, Saxena AK, Tiwari CM, Tiwari SK. Intensity variation of large solar energetic particle events associated with coronal mass ejections during Solar Cycle 24. Journal

of Informetrics. 2026a;20(1):68-78. doi:10.14148.JOI.2026.V20.I1.206.
8. Dwivedi R, Tiwari CM, Tiwari SK. Interplanetary propagation of solar energetic particles and the resulting modulation of galactic cosmic rays during Solar Cycle 25. International Journal of Physics and Applications. 2026b;8(1):192-199. doi:10.33545/26647575.2026.v8.i1b.261.
9. Echer E, Gonzalez WD, Tsurutani BT, Gonzalez ALC. Interplanetary conditions causing geomagnetic storms (Dst ≤ -100 nT) during solar cycle 23 (1996-2006). Journal of Geophysical Research. 2008b;113:A05221.
10. Gonzalez WD, Tsurutani BT. Criteria of interplanetary parameters causing intense magnetic storms (Dst <100 nT). Planetary and Space Science. 1987;35:1101-1109.
11. Gonzalez WD, Joselyn JA, Kamide Y, *et al*. What is a geomagnetic storm? Journal of Geophysical Research. 1994;99(A4):5771-5792.
12. Gonzalez WD, Tsurutani BT, Gonzalez ALC, Smith EJ, Tang F, Akasofu SI. Solar wind-magnetosphere coupling during intense magnetic storms (1978-1979). Journal of Geophysical Research. 1989;94:8835-8851.
13. Hapgood MA. Prepare for the coming space weather storm. Nature. 2012;484:311-313.
14. Hodgson R. On a curious appearance seen in the Sun. Monthly Notices of the Royal Astronomical Society. 1859;20:15-16.
15. Iyemori T. Storm-time magnetospheric currents inferred from midlatitude geomagnetic field variations. Journal of Geomagnetism and Geoelectricity. 1990;42:1249-1265.
16. Kamide Y, Yokoyama N, Gonzalez W, Tsurutani B, Daglis I, Brekke A, *et al*. Two-step development of geomagnetic storms. Journal of Geophysical Research. 1998;103:6917-6921.
17. Kataoka R, *et al*. The 17 March 2015 storm: The associated magnetic cloud and its geoeffectiveness. Earth, Planets and Space. 2015;67:79.
18. Lakhina GS, Alex S, Tsurutani BT, Gonzalez WD. Supermagnetic storms: hazard to society. In: Sharma AS, Bunde A, Dimri VP, Baker DN, editors. Extreme Events and Natural Hazards: The Complexity Perspective. Geophysical Monograph Series. Vol. 196. Washington: AGU; 2012. p. 267.
19. Loomis E. On the great auroral exhibition of Aug 28th-Sept 4, 1859, and on auroras generally. American Journal of Science. 1861;82:318.
20. Maurya K, Singh GN, Tiwari CM, Tiwari SK. Geomagnetic field and coronal mass ejections from 2019 to 2025. International Journal of Physics and Applications. 2026;8(1):26-30. doi:10.33545/26647575.2026.v8.i1a.230.
21. National Research Council Report. Severe Space Weather Events—Understanding Societal and Economic Impacts. Washington: National Academies Press; 2008.
22. Navia CE, Oliveira MNd, Augusto CRA. The highest geomagnetic storms of the solar cycle observed at ground level. In: Extreme Weather. InTech; 2018.
23. Rawat R, Echer E, Gonzalez WD. How different are the solar wind-interplanetary conditions and the consequent geomagnetic activity during the ascending and early descending phases of solar cycles 23 and 24? Journal of Geophysical Research: Space Physics. 2018;123(8):6621-6638.
24. Richardson IG. Energetic particles and coronal mass ejections. Space Science Reviews. 2004;111:267-376.
25. Richardson IG. Geomagnetic activity during the rising phase of solar cycle 24. Journal of Space Weather and Space Climate. 2013;3:A08.
26. Richardson IG, Cane HV. Near-Earth interplanetary coronal mass ejections during Solar Cycle 24. Solar Physics. 2012;281:187-222.
27. Rostoker G, Falthammar CG. Relationship between changes in the interplanetary magnetic field and variations in the magnetic field at the Earth's surface. Journal of Geophysical Research. 1967;72:5853-5863.
28. Skoug RM, Gosling JT, Steinberg JT, McComas DJ, Smith CW, Ness NF, *et al*. Extremely high speed solar wind: 29-30 October 2003. Journal of Geophysical Research. 2004;109:A09102.
29. Tiwari CM, Ojha L, Pandey J, Parsai MK, Gautam D, Pandey A, *et al*. Influence of heliospheric solar wind features on periodic and transient cosmic ray variations across Solar Cycle 24. International Journal of Contemporary Research in Multidisciplinary. 2026a;5(3):27-36. doi:10.5281/zenodo.20036604.
30. Tiwari CM, Gautam D, Parsai MK, Tiwari SK. Effect of geomagnetic storms on space weather during the ascending phase of Solar Cycle 24. Physical Science International Journal. 2026b;30(3):19-29. doi:10.9734/psij/2026/v30i3942.
31. Tiwari SK, Tiwari CM, Tripathi L, Sharma D. Investigation of solar causes for the cosmic ray enhancement on May 11, 2024. International Journal of Physics and Applications. 2024;6(2):57-60. doi:10.33545/26647575.2024.v6.i2a.102.
32. Tsurutani BT, Meng CI. Interplanetary magnetic field variations and substorm activity. Journal of Geophysical Research. 1972;77:2964.
33. Tsurutani BT, Gonzalez WD, Gonzalez ALC, Guarnieri FL, Gopalswamy N, Grande M, *et al*. Corotating solar wind streams and recurrent geomagnetic activity: A

review. Journal of Geophysical Research. 1995a;111:A01305.
34. Tsurutani BT, Gonzalez WD, Gonzalez ALC, Tang F, Arballo JK, Okada M. Interplanetary origin of geomagnetic activity in the declining phase of the solar cycle. Journal of Geophysical Research. 1995b;100:21717-21733.
35. Tsurutani BT, Gonzalez WD, Tang F, Akasofu SI, Smith EJ. Origin of interplanetary southward magnetic field responsible for major magnetic storms near solar maximum (1978-1979). Journal of Geophysical Research. 1988;93:8519.
36. Tsurutani BT, Verkhoglyadova OP, Manucci AJ, Lakhina GS, Huba JD. Extreme changes in the dayside ionosphere during a Carrington-type magnetic storm. Journal of Space Weather and Space Climate. 2012;2:A05.
37. Watari S. Geomagnetic storms of March and June 2015 and their solar sources. Earth, Planets and Space. 2017;69:70.

About the Corresponding Author

Sandeep Kumar Tiwari is associated with the Department of Physics at Govt Model Science College. He is engaged in academic and research activities in the field of physics, with interests in scientific studies, teaching, and emerging developments in physical sciences and interdisciplinary research.